A Semi-Empirical Model for Mean Wind Velocity Profile of Landfalling Hurricane Boundary Layers

Reda Snaiki, Teng Wu*

Department of Civil, Structural and Environmental Engineering, University at Buffalo, State University of New York, Buffalo, NY 14126, USA

**Corresponding author. Email:* tengwu@buffalo.edu

Abstract: The existence of the super-gradient-wind region, where the tangential winds are larger than the gradient wind, has been widely observed inside the hurricane boundary layer. Hence, the extensively used log-law or power-law wind profiles under near-neutral conditions may be inappropriate to characterize the boundary layer winds associated with hurricanes. Recent development in the wind measurement techniques overland together with the abundance of data over ocean enabled a further investigation on the boundary layer wind structure of hurricanes before/after landfall. In this study, a semi-empirical model for mean wind velocity profile of landfalling hurricanes has been developed based on the data from the Weather Surveillance Radar-1988 Doppler (WSR-88D) network operated by the National Weather Service and the Global Positioning System (GPS) dropsondes collected by the National Hurricane Center and Hurricane Research Division. The proposed mathematical representation of engineering wind profile consists of a logarithmic function of the height z normalized by surface roughness z_0 (z/z_0) and an empirical function of z normalized by the height of maximum wind δ (z/δ). In addition, the consideration of wind direction in terms of the inflow angle is integrated in the boundary layer wind profile. Field-measurement wind data for both overland and over-ocean conditions have been employed to demonstrate the accuracy of simulation and convenience in use of the developed semi-empirical model for mean wind velocity profile of landfalling hurricanes.

Keywords: *Hurricanes; boundary layer; wind field; Doppler radar; Dropsondes; Landfall.*

1. Introduction

Hurricane-related natural hazards are notorious for inflicting significant damage to life and property through high winds, torrential rain and storm surge. The insured losses due to landfalling hurricanes have been increasing due partly to the changing climate and continued escalation of coastal population density (e.g., Czajkowski et al. 2011; Rappaport 2014). In general, a mature hurricane consists of four main regions, namely a boundary layer, a region above the boundary layer with no radial motion, an updraft region, and a quiescent eye (Carrier et al. 1971). Nevertheless, the most important region for engineering applications is the boundary layer zone where the dynamics and thermodynamics are usually independently examined, or weakly coupled (Snaiki and Wu 2017a). The existence of the super-gradient-wind region has been widely observed inside the hurricane boundary layer. The supergradient region, where the maximum wind exists, was attributed by Kepert (2001) and Kepert and Wang (2001) to the strong inward advection of angular momentum. While the log-law or power-law wind profiles under near-neutral conditions are extensively used in engineering practice, they may be inappropriate to characterize the boundary layer winds associated with mature hurricanes. Wang and Wu (2017) indicated that the utilization of power-law or logarithmic profile may result in underestimation of the wind load effects on tall buildings under the hurricanes. As the construction of high-rise structures continues to grow in the hurricane-prone areas, it is imperative to develop a mathematical representation of engineering wind profile that could take the supergradient region into account in the wind design to ensure target safety and performance levels of civil infrastructures (Franklin et al. 2003; Snaiki and Wu 2017a).

The hurricane boundary layer under marine conditions has been extensively investigated due to the large database collected from reconnaissance aircraft, Stepped Frequency Microwave

Radiometer, moored buoy, ships data, and the Global Positioning System (GPS) dropsondes (e.g., Powell and Black 1990; Powell et al. 2003; Uhlhorn et al. 2007; Vickery et al. 2009). The National Oceanic and Atmospheric Administration (NOAA) started deploying GPS dropsondes in 1997 to collect dynamic and thermodynamic data from the hurricanes. The composite analysis based on the GPS dropsonde data was employed by a number of researchers to inspect the vertical profile of the mean wind speed inside the boundary layer region (e.g., Franklin et al. 2003; Powell et al. 2003; Vickery et al. 2009). Franklin et al. (2003) and Powell et al. (2003) observed the existence of a supergradient region characterized by a wind maximum in the eyewall region of the hurricane boundary layer. They also noted a logarithmic increase of the mean wind speed profiles from the surface to the height of the supergradient region, whereas the wind speeds decrease above the supergradient region due to the weakening of the horizontal pressure gradient (Franklin et al. 2003; Snaiki and Wu 2017b). The studies by Kepert (2001) and Kepert and Wang (2001) indicated that the height of maximum wind actually decreases with the increase of wind speed. A pronounced supergradient region near the radius of maximum winds was also highlighted by Vickery et al. (2009) using the GPS dropsondes data from 1997 to 2003. In addition, it was found that the lower few hundred meters of the boundary layer can be well represented by the classical log-law profile. Accordingly, Vickery et al. (2009) introduced a logarithmic-quadratic hurricane boundary layer model for vertical mean wind speed profile, where the lower and upper altitudes are normalized using the roughness length and boundary-layer height, respectively. The hurricane boundary layer wind model in Vickery et al. (2009) is best suited for marine conditions. Giammanco et al. (2013) also demonstrated the applicability of the log-law wind profile below the region of supergradient winds by examining the data from 1997 to 2005.

71 Although the implementation of GPS dropsondes has provided a rich source of data for the
72 investigation of hurricane vertical mean wind profile, it is essentially restricted to the marine
73 conditions. The landfalling hurricane dropsonde data is scarce due to the limited inland
74 observations. The conventional approach to acquire the landfall wind data using the portable
75 towers is limited in terms of vertical coverage and hence cannot capture the supergradient region
76 (e.g., Schroeder and Smith 2003; Schroeder et al. 2009; Masters et al. 2010). The Weather
77 Surveillance Radar-1988 Doppler (WSR-88D) network operated by the National Weather Service,
78 on the other hand, offers more flexibility to thoroughly examine the hurricane wind profiles over
79 land conditions. Based on the Velocity Azimuth Display (VAD) technique (Lhermitte and Atlas
80 1961; Browning and Wexler 1968), the mean velocity is represented by a function of azimuthal
81 angle for each conical scan at a constant elevation. Giammanco et al. (2012; 2013) used the WSR-
82 88D retrieved data to examine the boundary layer vertical mean wind profile overland based on
83 the VAD method. To avoid the challenges in the determination of gradient wind speed
84 (Willoughby 1990; Powell et al. 2003; Vickery et al. 2009), Giammanco et al. (2013) used the
85 mean boundary layer (MBL) wind speed, defined as the mean wind speed averaged over a height
86 range of 10 m to 500 m according to Powell et al. (2003), to normalize the wind profiles. The wind
87 maxima below the gradient wind region was clearly identified near the radius of maximum winds.
88 In addition, the height of supergradient region was observed to increase with the radial distance
89 from storm center. To generate wind profiles for landfalling hurricanes, Krupar (2015) employed
90 a refined VAD technique to further investigated the inland data between 1995 and 2012. Roughly
91 21,000 VAD wind profiles have been constructed in Krupar (2015) based on 20 WSR-88D radars
92 distributed along the United States coastlines to comprehensively explore the vertical and
93 horizontal wind distributions inside the hurricanes. He et al. (2013), on the other hand, identified

the supergradient region at around 500-600m height based on the wind measurements from a Doppler radar profiler and an anemometer. The existence of the supergradient winds of several typhoons were also reported by Tse et al. (2014a, 2014b) utilizing measurement data taken by a Doppler sodar and a boundary layer wind profiler.

In this study, a semi-empirical model for mean wind velocity profile of landfalling hurricanes has been developed based on the data from the WSR-88D network operated by the National Weather Service and the GPS dropsondes collected by the National Hurricane Center and Hurricane Research Division. The collected GPS dropsonde and WSR-88D wind data were re-analyzed to qualitatively and quantitatively characterize the hurricane boundary layer wind profiles over the open-ocean and inland conditions. It was conjectured that the structure of hurricane boundary layer winds is essentially determined by three parameters: surface shear stress τ_w, roughness length z_0 and height of the maximum wind δ. Accordingly, the proposed mathematical representation of engineering wind profile consists of a logarithmic function of the height z normalized by surface roughness z_0 (z/z_0) and an empirical function of z normalized by the height of maximum wind δ (z/δ). The developed hurricane boundary layer wind profile integrates the consideration of wind direction in terms of the inflow angle. The proposed semi-empirical model for mean wind velocity profile of hurricanes was validated based on the observation data from hurricanes Wilma and Katrina. Then, two case studies corresponding to the marine and landfalling conditions, respectively, have been utilized to highlight its applicability, due to high accuracy of simulation and convenience in use, to the wind design practice.

2. Wind Data Sources

2.1 GPS dropsondes

The GPS dropsondes, first deployed in 1997, are usually launched from an altitude of 1.5-3 km with a fall speed between 10-15 m/s (Hock and Franklin 1999). The dropsonde database established by the National Hurricane Center and Hurricane Research Division has provided a large number of high-resolution kinematic and thermodynamic profiles. Several studies examined the mean wind structure of hurricane boundary layer based on the composite profiles, where a large number of GPS dropsonde data were employed (e.g., Franklin et al. 2003; Powell et al. 2003; Vickery et al. 2009). Figure 1 depicts the GPS dropsonde data collected from 1996 to 2012, which have been utilized in the current study. As shown in Fig. 1(a), the selected data were restricted within a 300 km radius from the hurricane center to distinguish between the hurricane and environmental wind profiles. In addition, the GPS dropsondes that failed to gather data below 200 m were excluded. A total of 2120 dropsonde measurements used here, as illustrated by Fig. 1(b), are actually evenly distributed in the azimuthal direction of the hurricanes [Fig. 1(a)].

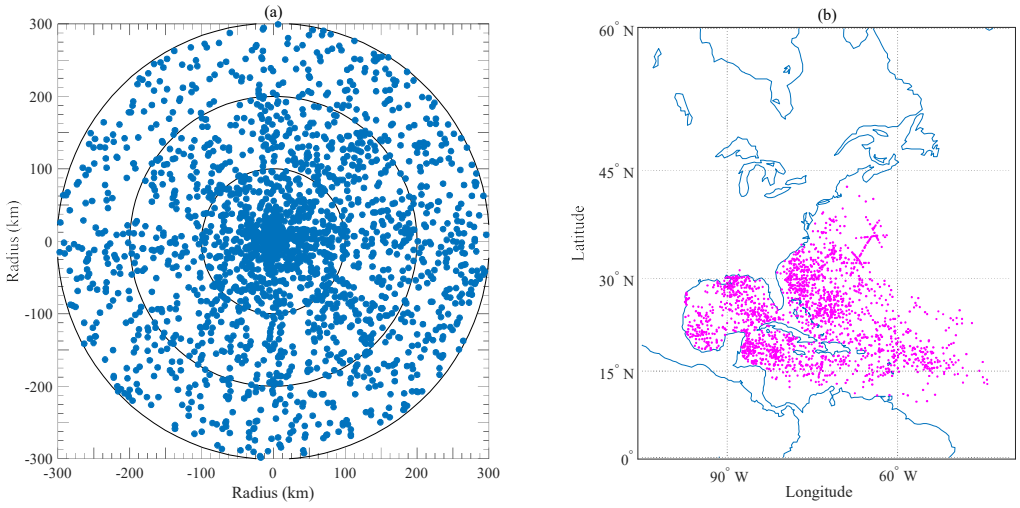

Fig. 1. GPS dropsonde data used in this study: (a) Azimuthal coverage of dropsonde data relative to hurricane center; (b) Location of selected dropsondes

The composite wind profiles were generated with the 2120 collected data following the approach adopted by Powell et al. (2003). The obtained profiles were then grouped according to

the MBL wind speed of 20-29, 30-39, 40-49, 50-59, 60-69, and 70-85 m/s. These six groups were ordered vertically into height bins, as illustrated in Fig. 2(a). More specifically, 10-m bins was selected for heights less than 300 m, 20-m for heights between 300 m and 500 m, 50-m for heights between 500 m and 1000 m, and 100-m for heights greater than 1000 m (Vickery et al. 2009). Figure 2(a) indicates that the profiles exhibit a logarithmic part up to the maximum wind speed (supergradient region) and its height decreases with increase of MBL wind speed (Powell et al. 2003; Vickery et al. 2009; Giammanco et al. 2013). The composite wind profiles were also presented in terms of the storm radius *r* associated to dropsonde data, as depicted by Fig. 2(b). As shown in the figure, the height of maximum wind generally increases with the storm radius. It is noted that the averaging time of the composite wind profile obtained from the GPS dropsondes can be assumed to roughly correspond to a 10-min or higher duration (Vickery et al. 2009).

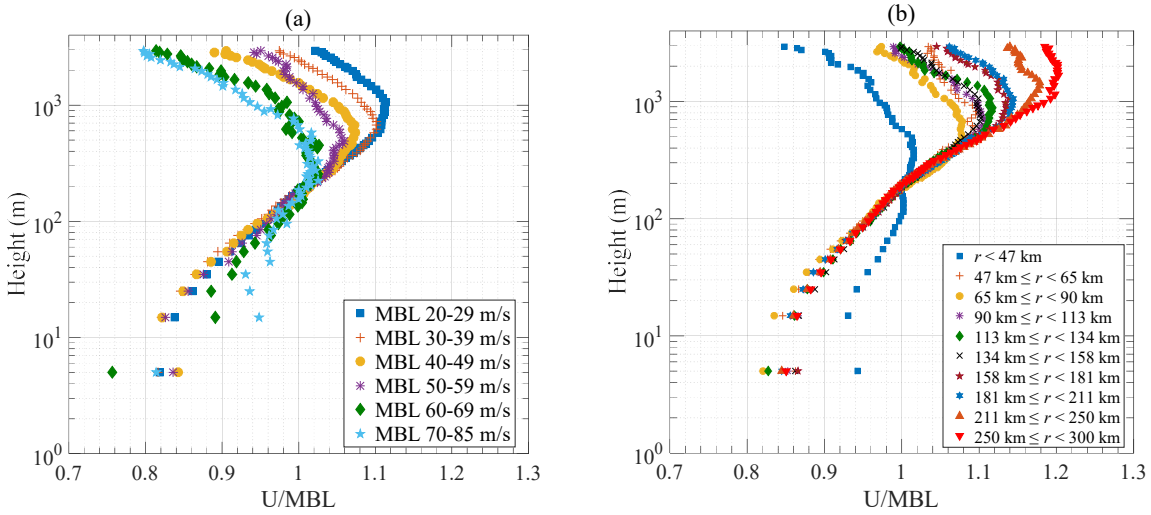

Fig. 2. Composite dropsonde wind profiles grouped by: (a) MBL wind speed and (b) storm radius

2.2 WSR-88D system

The WSR-88D system operated by the National Weather Service is a Doppler Radar consisting of several basic instruments, namely the radar product generator, the radar data acquisition and the

principal user processor. There are totally 155 WSR-88Ds in the United States, and the distribution of WSR-88D network used in the current study is presented in Fig. 3. Weather data, such as the wind speed and direction are obtained from WSR-88D based on the returned energy principle where the radar receives the reflected signal first transmitted in the form of a burst energy.

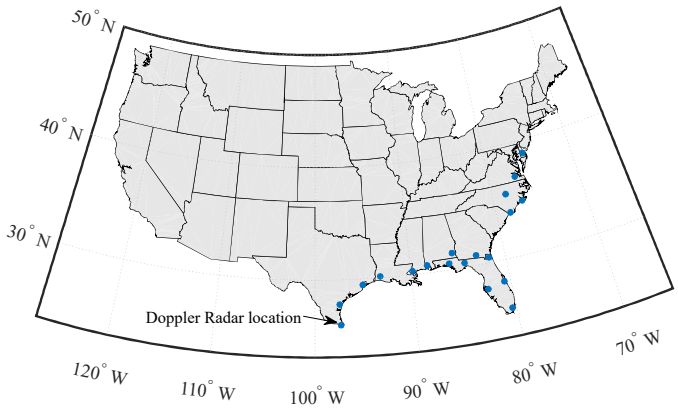

Fig. 3. WSR-88D network used in this study

Krupar (2015) constructed the mean structure of landfalling hurricane boundary layer winds based on the WSR-88D data from 34 hurricanes occurred from 1995 to 2012. The VAD technique-based vertical wind profiles were obtained with the height bins of a 50-m resolution below the 400 m, 75-m between 400 m and 700 m and 100-m above the 700 m. The VAD domain in the composite analysis was restricted to those data in the range of 3-5 km from the radar site (Giammanco et al. 2012; Giammanco et al. 2013; Krupar 2015). Figure 4(a) illustrates the normalized composite VAD horizontal wind speed profiles grouped by MBL wind speeds. Compared to Fig. 2(a) corresponding to the GPS dropsonde data, not all the obtained profiles from WSR-88D data present a pronounced super-gradient-wind region. More specifically, a wind maximum is observed only for wind profiles of groups 30-39 m/s and >40 m/s. Furthermore, the logarithmic profiles below the wind maxima in Fig. 4(a) show a faster decay of the wind speed towards the surface compared to the cases of dropsonde data. This observation suggests a more significant roughness length over land than that over the marine conditions (Giammanco et al.

2012). The VAD composite wind profiles were also grouped by storm radius, as depicted in Fig. 4(b). It is shown that the height of wind maximum increases with the storm radius. The minimum value of the obtained wind maximum heights is around 550 m that is higher than the one under marine conditions (Giammanco et al. 2013). It is noted that the averaging time of the VAD-derived wind profiles from WSR-88D data could be assumed to be a 10-min duration (Giammanco et al. 2012).

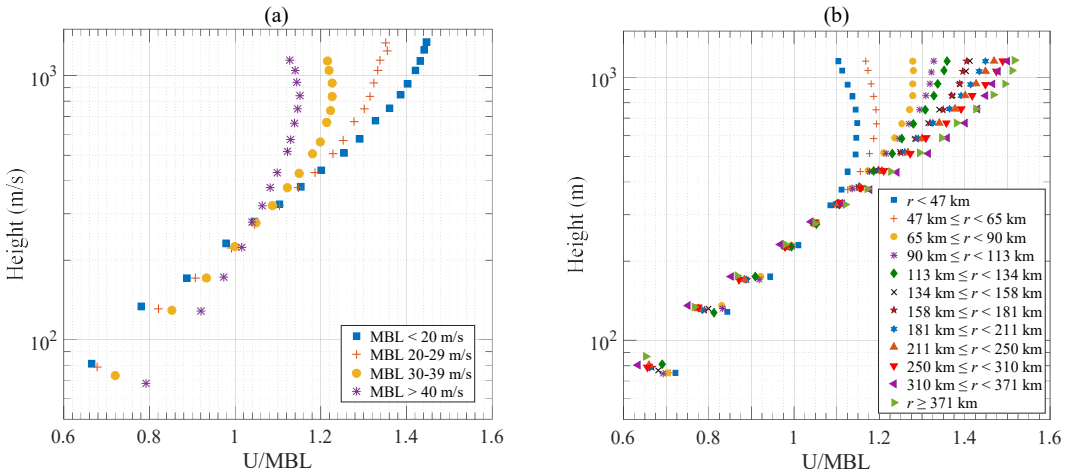

Fig. 4. VAD composite WSR-88D wind profiles grouped by (a) MBL wind speed and (b) storm radius [data from Krupar (2015)]

2.3 Data quality

The vertical profiles of wind speed were analyzed in a composite sense following the approach of Powell et al. (2003) and Vickery et al. (2009). Accordingly, it can be assumed that the wind speed samples are generated from a stationary process with an effective averaging time (~ 10 min) corresponding to a time scale long enough to filter out the non-stationary turbulent features inside the boundary layer (e.g., Powell et al. 2003; Vickery et al. 2009).

For the data from the GPS dropsondes, they were restricted within a 300 km radius from the hurricane center to ensure the obtained mean profiles are from the hurricane winds. The

189 hurricane boundary layer wind field over ocean is actually under the near-neutral conditions as
190 indicated by a number of researchers (e.g. Zhang et al. 2009), which means that the thermal effects
191 can be ignored. It should be mentioned that the collected data has been subjected to a quality
192 control by the National Hurricane Center and Hurricane Research Division to remove possible
193 errors and noises (using a 5-s low-pass filter) (Vickery et al. 2009).

194 For the data from the WSR-88D system, the VAD domain in the composite analysis was
195 restricted to those data in the range of 3-5 km from the radar site (Giammanco et al. 2012;
196 Giammanco et al. 2013; Krupar 2015). Since the thermodynamic measurements are not available
197 for the landfalling scenario through the Doppler radar, the "cut-off" approach popularly adopted
198 in the literature (e.g., Tse et al. 2013; He et al. 2016; Shu et al. 2017) was utilized here to eliminate
199 the effects of thermal instability on the wind measurements. Consequently, only the profile with a
200 MBL wind speed exceeding 10 m/s was retained in this study. Actually, the lower part of the
201 vertical wind profiles based on the collected data presents a logarithmic shape that is consistent
202 with a near-neutral stability surface layer, where the vertical distribution of momentum is
203 controlled by surface roughness (e.g., Giammanco et al. 2012; Giammanco et al. 2013).

204 **3. Wind Velocity Profile**

205 The wind data analyzed in Sect. 2 indicate that the large-scale wind features of hurricane boundary
206 layer may be essentially governed by three layers, namely lower part of surface friction, upper part
207 of the free atmosphere and middle part of supergradient winds. While the lower and upper parts
208 can be well described by the logarithmic solution and geostrophic wind relation, respectively, the
209 super-gradient wind mechanism needs further examination. Kepert and Wang (2001) suggested
210 that the supergradient winds may be attributed to the strong inward advection of the absolute

angular momentum (i.e., $M_a = rv + fr^2/2$ where f = Coriolis parameter and v = azimuthal wind component). According to $v = M_a/r - fr/2$, a high absolute angular momentum will lead to a substantial increase of the tangential wind component. The increase of the absolute angular momentum is maintained through the radial advection of momentum as well as the vertical diffusion and vertical advection of the radial winds. As a result, the maximum winds usually occur in the eyewall region where the updraft is substantial compared to other regions (e.g., Kepert 2001; Kepert and Wang 2001; Franklin et al. 2003; Powell et al. 2003). The supergradient wind actually corresponds to a positive net radial force field defined as $F_{sum} = -\frac{1}{\rho}\frac{\partial p}{\partial r} + \frac{v^2}{r} + fv$ (i.e., $F_{sum} > 0$), suggesting a higher value of the sum of Coriolis and centrifugal forces compared to the inwards radial pressure gradient. The upward advection of the inward momentum weakens beyond the supergradient wind region, therefore, the gradient imbalance $(F_{sum} \neq 0)$ can cause outflow that reduces the supergradient flow (Smith et al. 2009). As a result, the gradient balance $(F_{sum} = 0)$ is achieved on the top of the hurricane boundary layer. It is noted that the computationally-efficient linear wind field model typically neglects the vertical advection of the radial winds (e.g., Meng et al. 1995; Kepert 2001; Snaiki and Wu 2017a), hence, it usually underestimates the supergradient winds. Despite a number of discussions on the mechanism of supergradient region, a close-form solution for the middle-layer winds had never been done. Hence, an empirical patching between the lower logarithmic-law layer and upper geostrophic-balance layer will be utilized here.

3.1 Wind speed

3.1.1 Semi-empirical wind speed profile

231 The *v*-momentum equation of hurricane winds from the Navier-Stokes equations will be revisited
232 to determine a general expression of the azimuthal wind component *v*. Accordingly, the *v*-
233 momentum equation can be written in the cylindrical coordinate system (r,θ,z) as:

234 $$\frac{1}{\rho}\frac{\partial \tau^v}{\partial z} = u\frac{\partial v}{\partial r} + \frac{v}{r}\frac{\partial v}{\partial \theta} + w\frac{\partial v}{\partial z} + \frac{uv}{r} + fu \quad (1)$$

235 where (u,v,w) = wind velocity components; τ^v = shear stress in the azimuthal direction; ρ = air
236 density; and f = Coriolis parameter. Integrating Eq. (1) from the surface to a height z leads to the
237 following:

238 $$\frac{1}{\rho}\int_0^z \frac{\partial \tau^v}{\partial z} dz = \int_0^z \left(u\frac{\partial v}{\partial r} + \frac{v}{r}\frac{\partial v}{\partial \theta} + w\frac{\partial v}{\partial z} + \frac{uv}{r} + fu \right) dz \quad (2)$$

239 Hence, the shear stress can be obtained as:

240 $$\tau^v = \tau_w^v + \rho\int_0^z \left(u\frac{\partial v}{\partial r} + \frac{v}{r}\frac{\partial v}{\partial \theta} + w\frac{\partial v}{\partial z} + \frac{uv}{r} + fu \right) dz \quad (3)$$

241 where τ_w^v = the surface shear stress in the azimuthal direction. Based on the eddy viscosity model
242 of the shear stress, τ^v becomes:

243 $$\tau^v = \rho K_m \frac{dv}{dz} \quad (4)$$

244 where K_m = the eddy viscosity. K_m can be related to the frictional velocity (u_{*_v}) by using the
245 mixing-length hypothesis of $K_m = \kappa u_{*_v} z$ where κ is the von Karman constant. On the other hand,
246 the surface shear stress can be expressed as $\tau_w^v = \rho u_{*_v}^2$. Therefore, Eq. (3) becomes:

247 $$\frac{dv}{dz} = \frac{u_{*_v}}{\kappa z} + \frac{u_{*_v}}{\kappa}\left(\frac{\kappa^2 z}{K_m^2}\int_0^z \left(u\frac{\partial v}{\partial r} + \frac{v}{r}\frac{\partial v}{\partial \theta} + w\frac{\partial v}{\partial z} + \frac{uv}{r} + fu \right) dz \right) \quad (5)$$

248 The integration of Eq. (5) leads to the following result:

$$v(z) = \frac{u_{*v}}{\kappa}\left[\ln\left(\frac{z}{z_0}\right) + F(z)\right] \tag{6}$$

The function $F(z)$ in Eq. (6) actually represents the deviation part from the logarithmic profile. Since the azimuthal wind is the dominant component, similar formula of Eq. (6) will be adopted here for the horizontal mean wind speed (e.g., Giammanco et al. 2013; Krupar 2015). It is expected that $F(z)$ may possess two major components (terms) representing supergradient and gradient wind regions and the height z of the corresponding universal forms will be normalized by the height of maximum wind δ and gradient wind height H, respectively. To simplify the semi-empirical model of the hurricane boundary layer winds, however, the upper layer is removed in the engineering formula by limiting its applicable range to the height governed by the gersotrophic winds (see Sect. 3.1.2). In addition, a modified Ekman-like parametrization (product of the sine and/or cosine-type function with an exponential function) (e.g., Smith 1968; Langousis et al. 2009) is utilized to characterize the middle layer of supergradient winds and to empirically patch the lower and upper layers. Therefore, the proposed semi-empirical wind speed profile is presented as follows:

$$U_m(z) = \frac{u_*}{\kappa}\left[\ln\left(\frac{z}{z_0}\right) + \eta_0 \sin\left(\frac{z}{\delta}\right)\exp\left(-\frac{z}{\delta}\right)\right] \tag{7}$$

where $U_m(z)$ = mean wind speed as a function of height z; κ = von Karman constant; u_* = friction velocity; z_0 = surface roughness; δ = height of the maximum wind; and η_0 = a constant determined by the requirement of $\partial U_m / \partial z\big|_{z=\delta} = 0$, which leads to $\eta_0 \approx 9.026$. The logarithmic term of Eq. (7) can be replaced by the power-law distribution for more convenient engineering applications, as presented in Appendix A. The estimation of friction velocity u_* and roughness length z_0 is not

necessary in the empirical wind speed profile of Eq. (A.1). It should be noted that the proposed wind profile of Eq. (7) or Eq. (A.1) can consider the asymmetries due to the translation speed (integrated in the gradient wind) and surface roughness in the hurricane wind field distribution.

3.1.2 Applicable range of semi-empirical wind speed profile

The zero-plane displacement *d*, related to the average height of surface obstacles, is typically set as the lower limit of the boundary layer wind model (e.g., Meng et al. 1995; Tse et al. 2013; Snaiki and Wu 2017a). On the other hand, the upper limit of the developed semi-empirical wind profile z_i, related to the gradient wind height, cannot be obtained straightforwardly. The wind speed at gradient level is expected to decrease due to the weakening of the radial pressure gradient, however, the determination of the height at which the gradient balance occurs is actually challenging (e.g., Powell et al. 2003). The hurricane gradient wind height *H* could be between 1km and 3km (e.g., Willoughby 1990; Powell et al. 2003). Based on the field-measurement data, it is reasonable to assume that there is a linear overlap function between the supergradient and gradient wind regions. Hence, the upper limit z_i could be determined to ensure a smooth transition between these two regions. The slope associated to the semi-empirical wind profile at a starting height of $z_i = \delta + \Delta\delta$ could be computed as $s_1 = \left.\partial U_m \middle/ \partial z\right|_{z_i=\delta+\Delta\delta}$ where $\Delta\delta$ is the height increment (e.g., 10 m). On the other hand, the slope associated to the overlap region will be $s_2 = \left[v_g - U_m(z_i)\right] \middle/ \left(H - z_i\right)$. This upper limit z_i will be determined by setting $s_1 = s_2$, as illustrated in Fig. 5.

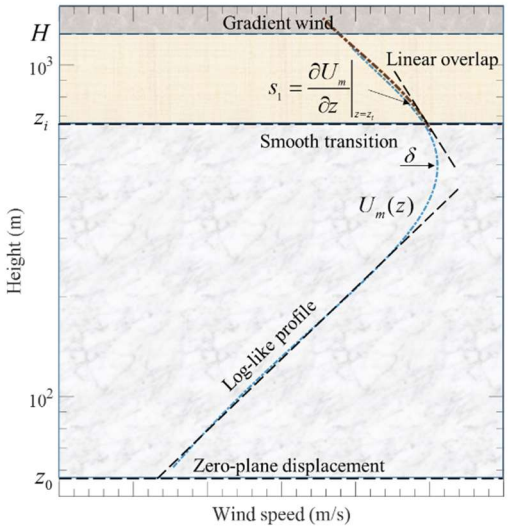

Fig. 5. Lower and upper limits of semi-empirical wind profile

3.1.3 Model fitness

The proposed semi-empirical hurricane boundary layer wind models of Eqs. (7) and (A.1) together with the logarithmic-quadratic model of Vickery et al. (2009) were used to fit the field-measurement data to represent the mean wind speed profiles. To this end, the wind data of tropical cyclones Floyd (1999) on September 16, Ike (2008) on September 13 and Molave (2009) on July 19 (Tse et al. 2013), covering both landfall and offshore scenarios, were utilized to test the fitness of these three models. The fitting results are presented in Fig. 6 and Table 1, where the Levenberg-Marquardt algorithm (Levenberg, 1944; Marquardt, 1963) is employed to minimize the squared difference between the observed data and numerical results. It can be seen from the fitting results that the height of maximum wind δ is almost identical for the profiles of Eq. (7) and Eq. (A.1), both of which are less than that from Vickery's profile. While the friction velocity u_* and surface roughness z_0 of the proposed semi-empirical model for Floyd, Ike, and Molave match the terrain exposure conditions (Powell et al. 2004; Tse et al. 2013), Vickery's model yielded unrealistically large values.

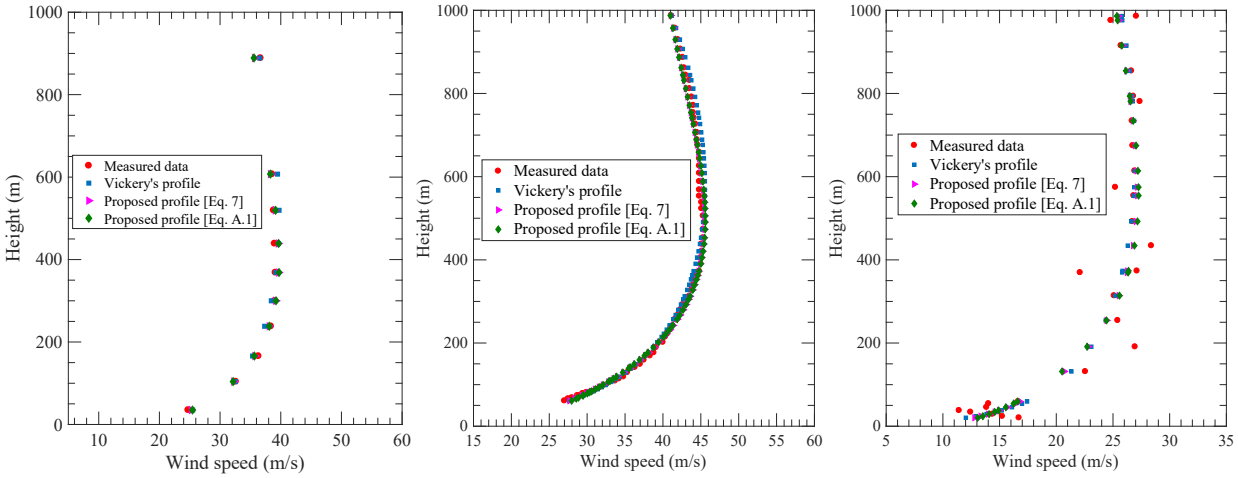

Fig. 6. Comparison between observed and fitted wind profiles for tropical cyclones Floyd (left), Ike (middle) and Molave (right)

Table 1. Fitting results of mean wind speed profiles for tropical cyclones Floyd, Ike and Molave

Tropical cyclone	Vickery's profile			Proposed profile [Eq. 7]			Proposed profile [Eq. A.1]		
	$u_*(m/s)$	$z_0(m)$	$\delta(m)$	$u_*(m/s)$	$z_0(m)$	$\delta(m)$	$U_{10}(m/s)$	α	$\delta(m)$
Molave	2.01	1.85	580.41	0.99	0.15	566.57	11.03	0.14	558.53
Ike	4.11	4.13	515.84	1.83	0.38	496.34	17.53	0.16	497.01
Floyd	2.62	0.72	451.05	1.29	0.03	393.19	19.90	0.11	393.37

3.2 Wind direction

In addition to the wind speed, the consideration of wind direction is essential in the examination of wind effects on the civil infrastructures. In this study, the wind direction is considered in terms of the inflow angle γ as illustrated by Fig. 7.

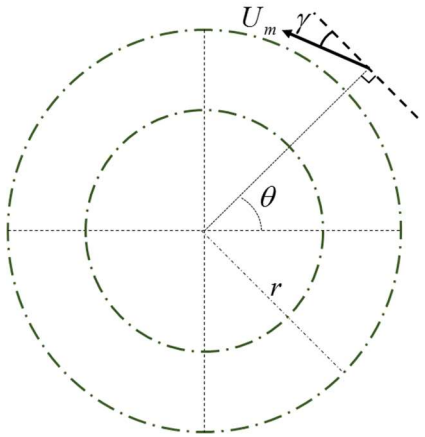

Fig. 7. Inflow angle definition

From the visual inspection of the vertical profiles of inflow angle γ for both marine and inland conditions (e.g., Fig. 8), γ decreases with increase of height. This pattern is reasonable as the surface friction effects, which substantially contribute to the inflow, are wakened with height. More specifically, the variation of γ in the boundary layer region could be approximately represented by a linear-like function of height with a various slope depending on the location inside the hurricane. Therefore, it is assumed that γ can be empirically expressed as:

$$\gamma(z) = \gamma_s \left| 1 - (\alpha + \beta r)\frac{z}{\delta} \right|^{\lambda} \tag{8}$$

where γ_s = surface inflow angle; and (α, β, λ) = constants empirically determined based on the fitting process of the measured data. To assess the goodness-of-fit, the R-squared value R_f^2 (also denoted as the coefficient of determination) is used in this study.

Two sets of constants in Eq. (8) are obtained based on the data from the dropsondes and WSR-88D network, as summarized in Table 2. The obtained values of R_f^2 for the dropsondes and for the WSR-88D are 0.92 and 0.95, respectively. Figure 8 depicts the comparison of the measured inflow angle and the fitted profiles for the marine and inland cases.

Table 2. Inflow angle parameters (The radius r in km)

Data source	Dropsondes data	WSR-88D data
α	0.075	0.6249
β	0.0022	0.0017
λ	1.17	1.17
γ_s	25°	Eq. (9)

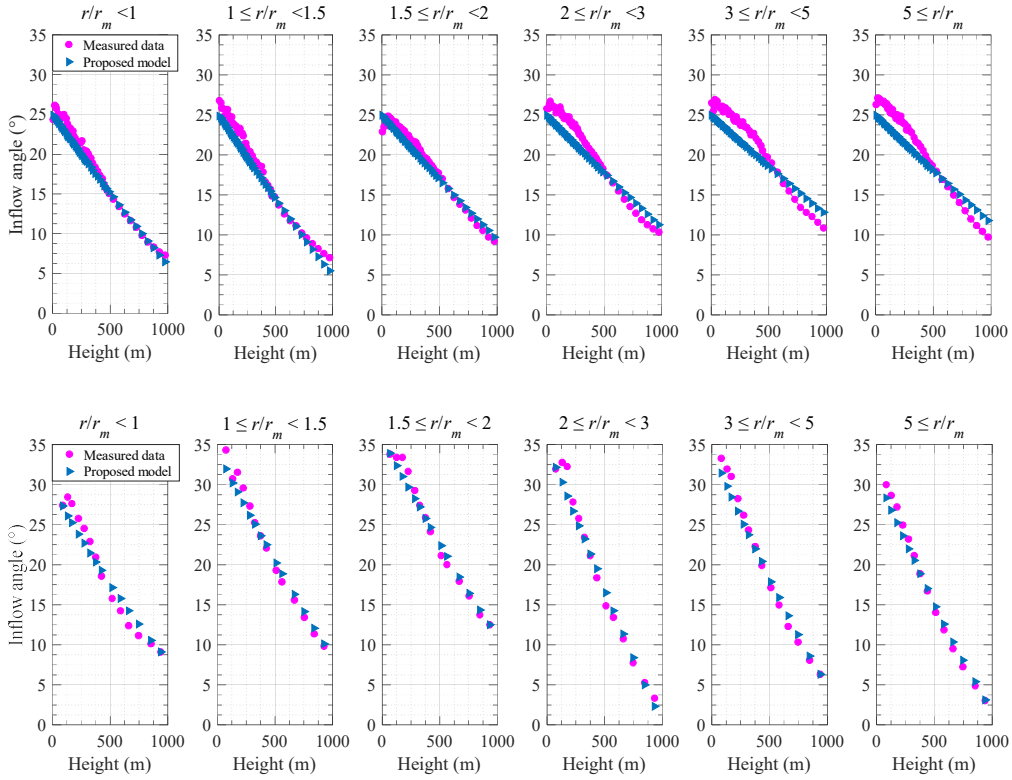

Fig. 8. Comparison of measured inflow angle and fitted profiles for the marine case (upper) and inland case (lower)

Extensive studies on γ_s for the marine conditions (e.g., Bretschneider 1972; Phadke et al. 2003; Zhang and Uhlhorn 2012) indicated that the γ_s is generally insensitive to the radial coordinate r (with an average value of $\gamma_s \approx 25°$). For the inland conditions, however, the γ_s significantly changes with respect to r. Zilitinkevich (1989) examined the surface roughness effects on the surface inflow angle for the case of a non-hurricane climate in terms of the surface Rossby number. Meng et al. (1996) extended the study of Zilitinkevich (1989) to the typhoon scenarios by introducing an additional non-dimensional parameter ξ characterizing the heterogeneity of the

vorticity in the radial direction. In this study, a similar parametrization scheme of Meng et al. (1996) is employed leading to the following expression:

$$\gamma_s = \left(A + B\xi\right)\left(\ln Ro_s\right)^C \tag{9}$$

where the constant coefficients A, B and C obtained by fitting WSR-88D data are 15, 80 and -0.6, respectively. The non-dimensional parameter ξ is defined as $\xi = \sqrt{\zeta_g / \zeta_{ag}}$ (where $\zeta_g = 2v_g / r + f$ and $\zeta_{ag} = \partial v_g / \partial r + v_g / r + f$) with ζ_g represents the absolute angular velocity and ζ_{ag} corresponds to the vertical component of absolute vorticity of the gradient wind v_g (Snaiki and Wu 2017b). The modified surface Rossby number Ro_s is defined as $Ro_s = v_g / Iz_0$, where the inertial stability I is given as $I = \sqrt{\left(f + 2v_g / r\right)\left(f + v_g / r + \partial v_g / \partial r\right)}$. The coefficient of determination R_f^2 is 0.83 between the measured data and numerical results of Eq. (9). On the other hand, a purely-empirical formula of γ_s can be proposed based on the inland data from the WSR-88D as:

$$\begin{cases} \gamma_s = 0.3148\left(\dfrac{r}{r_{\mathrm{m}}}\right)^3 - 3.9724\left(\dfrac{r}{r_{\mathrm{m}}}\right)^2 + 14.053\left(\dfrac{r}{r_{\mathrm{m}}}\right) + 21.49875 & 0 \le r \le 5.5r_{\mathrm{m}} \\ \gamma_s = 31^\circ & 5.5r_{\mathrm{m}} \le r \end{cases} \tag{10}$$

This purely-empirical formula of Eq. (10) is actually more convenient to be used since it requires only the radius of maximum winds to determine the surface inflow angle. The coefficient of determination between the measured data and numerical results of Eq. (10) R_f^2 is 0.95.

3.3 Parameter identification

The semi-empirical wind profile of Eq. (7) is a function of the unique independent variable z (height) and three external parameters δ (height of maximum wind), u_* (friction velocity) and z_0

360 (roughness length). The values of z_0 could be obtained in neutral stratification using several
361 widely-used schemes, such as classification tables (e.g., Wieringa 1992, 1993), ground-based
362 photography (e.g., Powell et al. 2004) or averages of neutrally stratified mean gust factors (Master
363 et al. 2010). In the case that z_0 is given, the friction velocity u_* could be estimated based on
364 $u_* = \kappa U_{10} \Big/ \ln\left(10/z_0\right)$ (e.g., Powell et al. 2003). Otherwise, both u_* and z_0 can be obtained through the
365 least squares fit of the measured vertical wind speed profile in the linear-logarithmic space. In
366 addition, u_* can be directly determined from its definition when accurate and reliable
367 measurements of the horizontal Reynolds stress vector are available (e.g., Weber 1999; Masters et
368 al. 2010).

369 Currently, a well-established approach to obtain the height of maximum wind in Eq. (7)
370 has not been developed yet. Kepert and Wang (2001) indicated that the linear height-resolving
371 model, although underestimates the magnitude of the supergradient winds, can be used to
372 effectively estimate the height of maximum wind. According to the linear theory, the height of
373 maximum wind is inversely proportional to the square root of the inertial stability $\sqrt{I}$ (e.g.,
374 Rosenthal 1962; Kepert 2001; Eliassen and Lystad 1977; Vickery et al. 2009; Snaiki and Wu
375 2017a). On the other hand, Vickery et al. (2009) claimed that the height scale can be better modeled
376 as a function of $1/I$ compared to that of $1/\sqrt{I}$. In addition, the contribution of surface roughness
377 corresponding to various terrain exposure conditions to the height scale should be integrated. As a
378 result, the height of maximum wind in this study is determined according to the following formula:

379 $$\ln\left(\delta\right) = a\ln\left(I\right) + b\ln\left(Ro_s\right) + c \tag{11}$$

380 where (a,b,c) = empirical constants. The fitting results of these constants based on the measured
381 data under the marine and inland conditions are presented in Table 3, with corresponding R-

squared values between measured and simulated heights of 0.77 and 0.87, respectively. A negative value of parameter a implies that δ is inversely proportional to the inertial stability, while a negative value of parameter b indicates that δ increases with the surface roughness. Figure 9 depicts the comparison of field-measured and numerically-calculated δs for both marine and inland cases, and good agreements are achieved.

Table 3. Parameters for the height of maximum wind

Data source	Dropsondes data	WSR-88D data
a	-0.4807	-0.2452
b	-0.05	-0.05
c	4.0221	5.6149

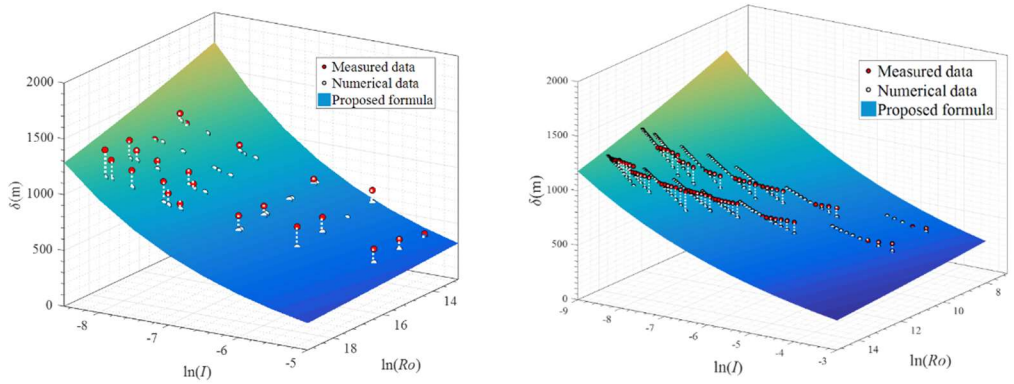

Fig. 9. Comparison of field-measured and numerically-calculated heights of maximum wind for (left) the marine case and (right) the inland case

3.4 Sensitivity Analysis

To more comprehensively examine the proposed semi-empirical model for the mean wind velocity profiles of hurricanes, the sensitivity analysis of the height of maximum wind $\ln(\delta)=a\ln(I)+b\ln(Ro_s)+c$, the surface inflow angle $\gamma_s=(A+B\xi)(\ln Ro_s)^C$ and the inflow angle $\gamma(z)=\gamma_s\left|1-(\alpha+\beta r)\frac{z}{\delta}\right|^{\lambda}$ was conducted, and presented in Fig. 10. The radial variation of the inertial stability I, surface Rossby number Ro_s and parameter ξ were determined based on the data from hurricane Katrina (2005) [to be detailed in the model validation (Sect. 4.1)]. It is shown that the

height of maximum wind δ is not sensitive to a, while b and c substantially alter its values. For the inflow angle $\gamma(z)$, α and β only slightly change its slope and λ marginally modifies its profile concavity. On the other hand, no significant change (a maximum value of $2°$) in the surface angle γ_s is observed for various values of A, B and C.

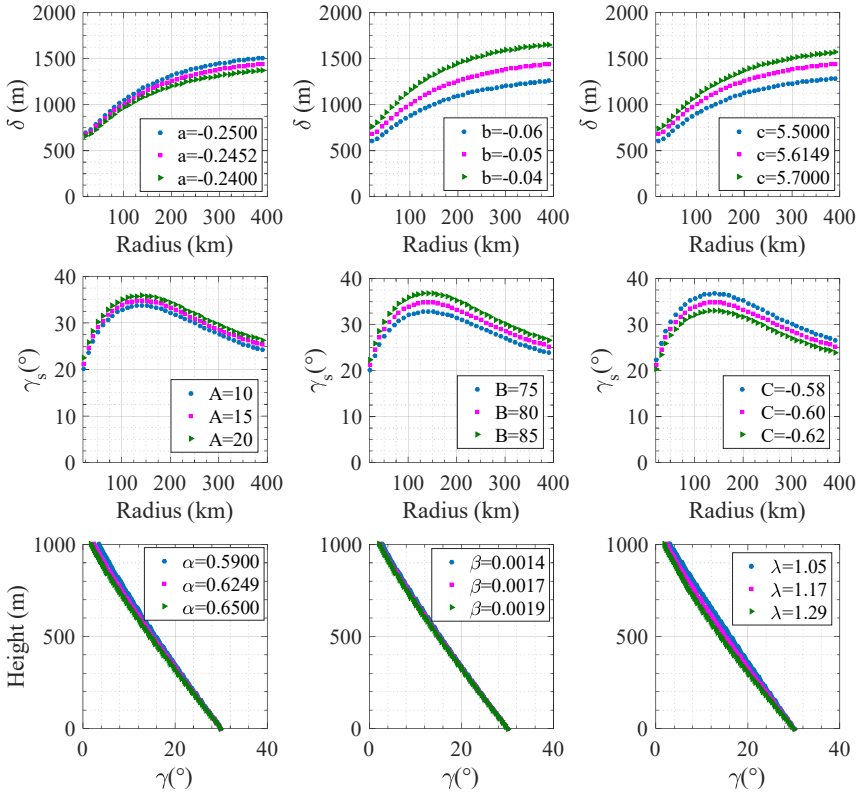

Fig. 10. Sensitivity analysis of proposed wind profile parameters

4. Model Validation and Application

4.1 Model validation

The developed semi-empirical model for hurricane mean wind velocity profile will be validated based on two scenarios, namely hurricane Wilma (2005) and hurricane Katrina (2005).

Hurricane Wilma had devastating damages on Cuba, Mexico and south Florida. It reached tropical Storm status on 17 October 2005 and became a hurricane on 18 October 2005. It was then intensified to Category 5 hurricane on 19 October with a maximum sustained surface wind of 82.3

m/s. The recorded minimum central pressure was 882 hpa. Wilma hit the southern Florida as a Category 3 hurricane. The comparison between the wind profiles, at the location of $\left(\mathrm{N25.61}^{\circ},\mathrm{W80.41}^{\circ}\right)$ corresponding to a landfalling case with the estimated surface roughness $z_0 \approx 0.1m$ using the Land Use Land Cover (e.g., Powell et al. 2004), measured from the Doppler radar KAMX and calculated based on the proposed semi-empirical model is depicted in Figure 11. The identified friction velocity u_* is 1.82 m/s and the height of maximum wind δ is 862.45 m. All other parameters needed in the simulation were obtained from the HURDAT database on 24 October at 1200 UTC. A good agreement between observed and simulated wind speeds and inflow angles is achieved.

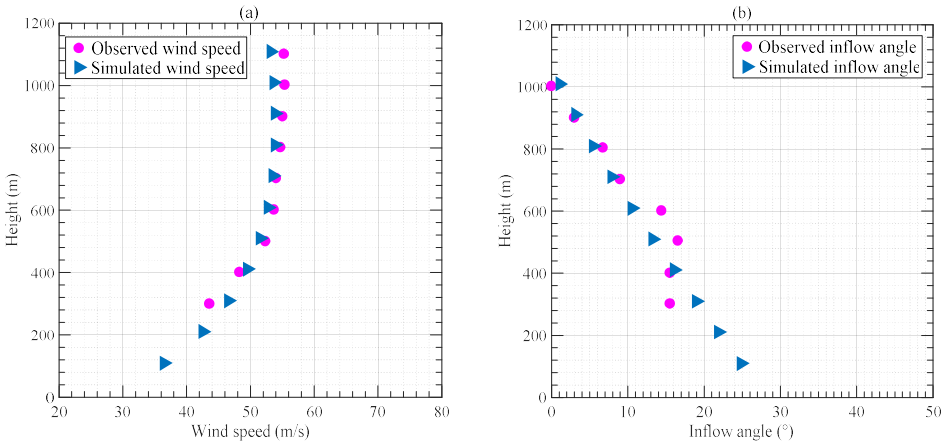

Fig. 11. Observed and simulated wind speed (a) and inflow angle (b) of Hurricane Wilma

Hurricane Katrina reached the Hurricane strength on 25 August 2005 at 2100 UTC, then crossed the southern Florida after making landfall near Miami at 2230 UTC. Katrina was intensified again after a weakening stage on the eastern coast of Florida to reach Category 5 hurricane on 28 August. It made another landfall near Buras, Louisiana on 29 August as a Category 3 hurricane. Figure 12 presents the comparison between the wind profiles provided by the KAMX Doppler radar and semi-empirical model at the location of $\left(\mathrm{N25.61}^{\circ},\mathrm{W80.41}^{\circ}\right)$, corresponding to a landfalling case with the estimated surface roughness $z_0 \approx 0.1m$. The identified friction velocity u_*

is 1.19 m/s and the height of maximum wind δ is 715.20 m. All other parameters needed in the simulation were obtained from the HURDAT database on August 26 at 0000 UTC. As shown in the figure, an excellent agreement between the observed and simulated wind speeds is observed. On the other hand, the simulated inflow angles show slight difference with the measurements.

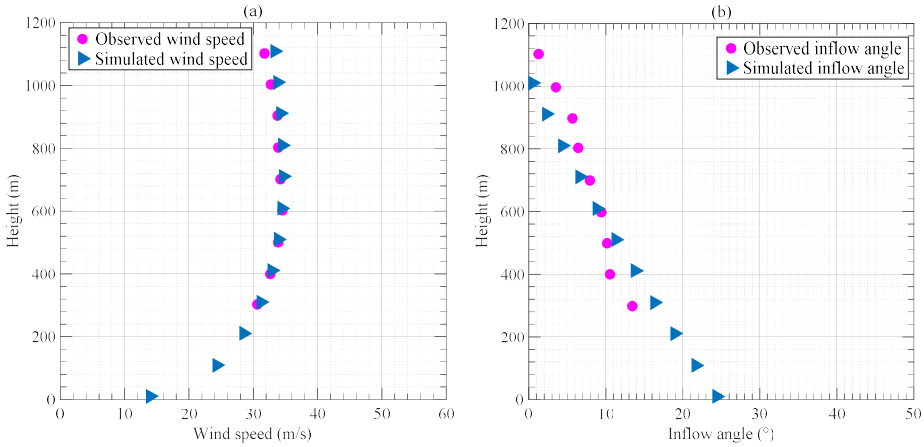

Fig. 12. Observed and simulated wind speed (a) and inflow angle (b) of Hurricane Katrina

4.2 Application

Two case studies corresponding to the overland and marine conditions, respectively, will be presented to highlight the simulation convenience and efficiency of the developed semi-empirical wind model. The hurricane parameters of these two scenarios for the wind field simulation are summarized in Table 4. The values of central pressure p_c, radius of maximum winds r_m, Holland *B* parameter, translational speed *c*, approach angle υ, and latitude and longitude (ψ,λ) in Table 4 are utilized to obtain the gradient wind, and then the gradient-to-surface wind reduction factors could be employed to derive the surface wind speed U_{10} for the estimation of the friction velocity u_* (e.g., Sparks and Huang 1999; Lee and Rosowsky 2007). With the values of z_0 listed on Table 4 and δ obtained using Eq. (11), the wind speed and direction can be obtained based on the

446 proposed formulas of Eq. (7) and Eq. (8), respectively. The simulation results under the inland and

447 marine conditions are illustrated in Fig. 13 and 14, respectively.

448 **Table 4.** Hurricane parameters for wind field simulation

Parameter	p_c (hpa)	r_m (km)	B	c (m/s)	υ(°)	ψ (°)	λ (°)	z_0 (m)
Inland scenario	965	50	1.3	8	90	39.73	-74.22	0.1
Marine scenario	940	50	1.3	8	90	29.77	-73.60	0.001

449

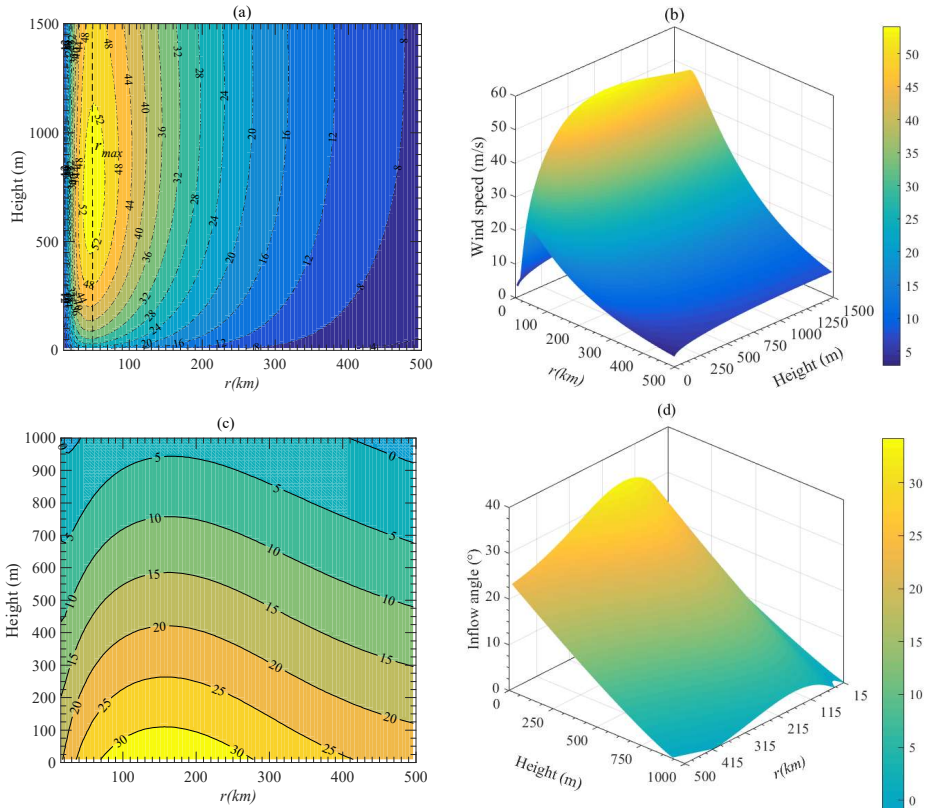

450

451

452 **Fig. 13.** Wind field simulation of inland scenario: (a) Contour of vertical wind speed; (b) Three dimensional shaded

453 surface of wind speed; (c) Contour of inflow angle; (d) Three dimensional shaded surface of inflow angle

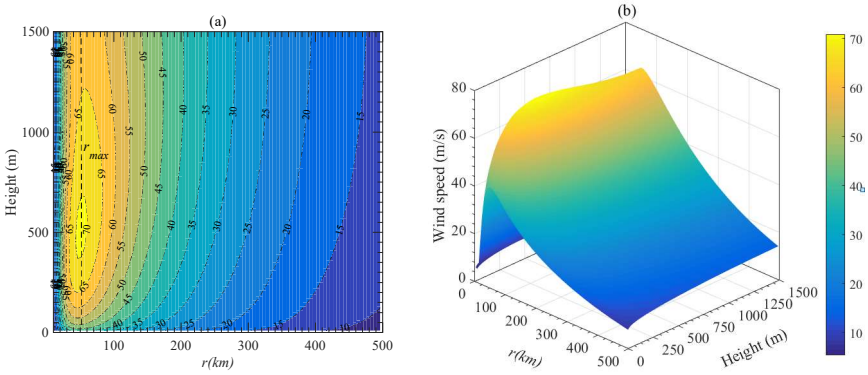

454

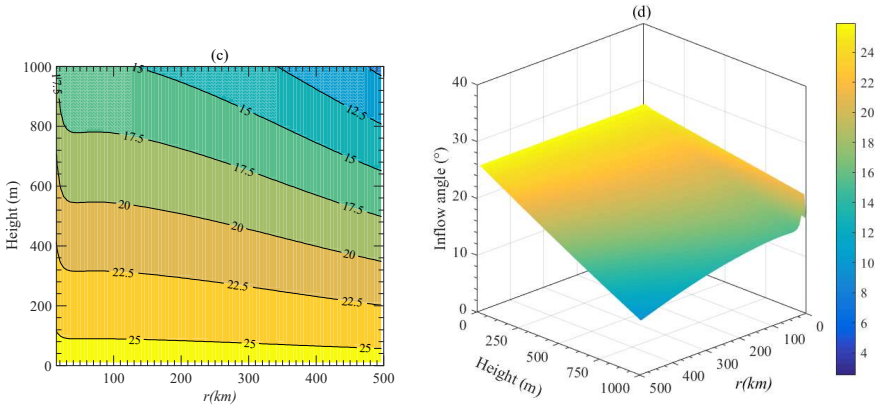

Fig. 14. Wind field simulation of marine scenario: (a) Contour of vertical wind speed; (b) Three dimensional shaded surface of wind speed; (c) Contour of inflow angle; (d) Three dimensional shaded surface of inflow angle

As shown in both Figs. 13 and 14, the supergradient region is clearly identified near the radius of maximum wind r_m while a log-like wind profile is obvious in the outer vortex region. The comparison between the landfalling and marine cases indicates that the height of maximum wind over ocean is lower than that over land. To more clearly present the abovementioned observations in Figs. 13 and 14, two wind profiles corresponding to the eye-wall (r = 50 km) and outer vortex regions (r = 200 km) were plotted in Fig. 15 for both inland and marine simulations. The existence of the super-gradient-wind region is highlighted inside the eyewall region. In addition, the height of maximum wind over ocean is around 460 m while the one over land is around 680 m.

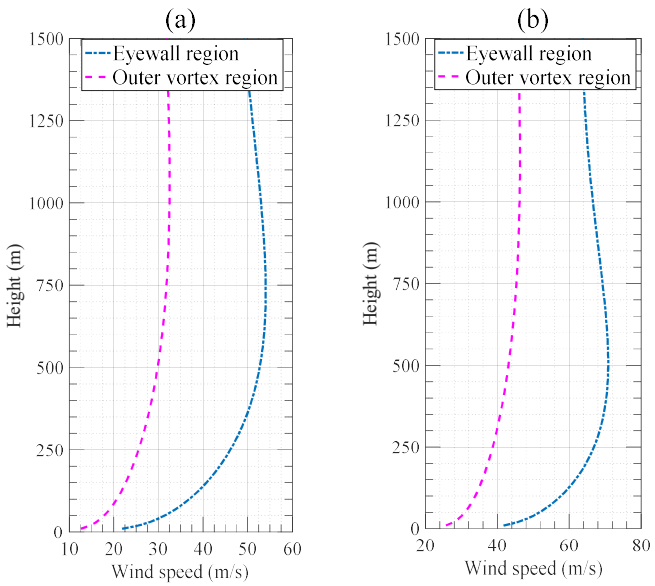

Fig. 15. Vertical wind profile of eyewall and outer vortex regions under (a) landfall condition; (b) marine condition

5. Concluding Remarks

A semi-empirical model for mean wind velocity profile of landfalling hurricanes has been developed based on the re-analysis of data from the Weather Surveillance Radar-1988 Doppler (WSR-88D) network and the Global Positioning System (GPS) dropsondes. The new mathematical representation of hurricane boundary layer wind profile consists of a logarithmic function of the height z normalized by surface roughness z_0 (z/z_0) and an empirical function of z normalized by the height of maximum wind δ (z/δ). The proposed engineering model for the height of maximum wind δ highlights the contribution from both the inertial stability and surface roughness. The fast and reliable estimation of δ facilitates the accuracy of simulation and convenience in use of the semi-empirical wind model. The consideration of wind direction in terms of the inflow angle further improves the applicability of the developed hurricane wind field model to the wind design practice. The new model may have a contribution to codification of the landfalling hurricane boundary layer wind field, especially in the consideration of super-gradient-wind region.

Acknowledgments

The support for this project provided by the NSF Grant # CMMI 15-37431 is gratefully acknowledged.

Appendix A

An empirical wind speed profile could be obtained by replacing the logarithmic term of Eq. (7) with the power-law distribution:

$$U(z) = U_{10}\left[\left(\frac{z}{10}\right)^{\alpha} + \eta_1 \sin\left(\frac{z}{\delta}\right)\exp\left(-\frac{z}{\delta}\right)\right] \tag{A.1}$$

where $\alpha =$ power law exponent; and the parameter η_1 is determined by setting $\partial U/\partial z\big|_{z=\delta} = 0$ resulting in the following expression:

$$\eta_1 = \frac{\left(\delta/10\right)^{\alpha}\alpha e}{\sin(1) - \cos(1)} \tag{A.2}$$

References

Bretschneider, C.L., 1972, January. A non-dimensional stationary hurricane wave model. In Offshore Technology Conference. Offshore Technology Conference.

Browning, K.A. and Wexler, R., 1968. The determination of kinematic properties of a wind field using Doppler radar. Journal of Applied Meteorology, 7(1), pp.105-113.

Carrier, G.F., Hammond, A.L. and George, O.D., 1971. A model of the mature hurricane. Journal of Fluid Mechanics, 47(1), pp.145-170.

Czajkowski, J., Simmons, K. and Sutter, D., 2011. An analysis of coastal and inland fatalities in landfalling US hurricanes. Natural hazards, 59(3), pp.1513-1531.

Eliassen, A. and Lystad, M., 1977. The Ekman layer of a circular vortex-A numerical and theoretical study. Geophysica Norvegica, 31, pp.1-16.

Franklin, J.L., Black, M.L. and Valde, K., 2003. GPS dropwindsonde wind profiles in hurricanes and their operational implications. Weather and Forecasting, 18(1), pp.32-44.

Giammanco, I.M., Schroeder, J.L. and Powell, M.D., 2012. Observed characteristics of tropical cyclone vertical wind profiles. Wind and Structures, 15(1), p.65.

509 Giammanco, I.M., Schroeder, J.L. and Powell, M.D., 2013. GPS dropwindsonde and WSR-88D observations of
510 tropical cyclone vertical wind profiles and their characteristics. Weather and Forecasting, 28(1), pp.77-99.

511 He, Y.C., Chan, P.W. and Li, Q.S., 2013. Wind profiles of tropical cyclones as observed by Doppler wind profiler and
512 anemometer. Wind and Structures, 17(4), pp.419-433.

513 He, Y.C., Chan, P.W. and Li, Q.S., 2016. Observations of vertical wind profiles of tropical cyclones at coastal areas.
514 Journal of Wind Engineering and Industrial Aerodynamics, 152, pp.1-14.

515 Hock, T.F. and Franklin, J.L., 1999. The ncar gps dropwindsonde. Bulletin of the American Meteorological Society,
516 80(3), pp.407-420.

517 Kepert, J., 2001. The dynamics of boundary layer jets within the tropical cyclone core. Part I: Linear theory. Journal
518 of the Atmospheric Sciences, 58(17), pp.2469-2484.

519 Kepert, J. and Wang, Y., 2001. The dynamics of boundary layer jets within the tropical cyclone core. Part II: Nonlinear
520 enhancement. Journal of the atmospheric sciences, 58(17), pp.2485-2501.

521 Krupar III, R.J., 2015. Improving surface wind estimates in tropical cyclones using WSR-88D derived wind profiles
522 (Doctoral dissertation).

523 Langousis, A., Veneziano, D. and Chen, S., 2009. Boundary layer model for moving tropical cyclones. In Hurricanes
524 and Climate Change (pp. 265-286). Springer, Boston, MA.

525 Lee, K.H. and Rosowsky, D.V., 2007. Synthetic hurricane wind speed records: development of a database for hazard
526 analyses and risk studies. Natural Hazards Review, 8(2), pp.23-34.

527 Levenberg, K., 1944. A method for the solution of certain non-linear problems in least squares. Quarterly of applied
528 mathematics, 2(2), pp.164-168.

529 Lhermitte, R., and D. Atlas, 1961. Precipitation motion by pulse Doppler radar. Proc. 9th Wea Radar Conf., Boston,
530 MA, Am. Meteor. Soc., 218-223.

531 Marquardt, D.W., 1963. An algorithm for least-squares estimation of nonlinear parameters. Journal of the society for
532 Industrial and Applied Mathematics, 11(2), pp.431-441.

533 Masters, F.J., Vickery, P.J., Bacon, P. and Rappaport, E.N., 2010. Toward objective, standardized intensity estimates
534 from surface wind speed observations. Bulletin of the American Meteorological Society, 91(12), pp.1665-1681.

535 Meng, Y., Matsui, M. and Hibi, K., 1995. An analytical model for simulation of the wind field in a typhoon boundary
536 layer. Journal of wind engineering and industrial aerodynamics, 56(2-3), pp.291-310.

537 Meng, Y., Matsui, M. and Hibi, K., 1996. Characteristics of the vertical wind profile in neutrally atmospheric boundary
538 layers. Part 2: Strong winds during typhoon climates. Journal of Wind Engineering, 1996(66), pp.3-14.

539 Phadke, A.C., Martino, C.D., Cheung, K.F. and Houston, S.H., 2003. Modeling of tropical cyclone winds and waves
540 for emergency management. Ocean Engineering, 30(4), pp.553-578.

541 Powell, M.D. and Black, P.G., 1990. The relationship of hurricane reconnaissance flight-level wind measurements to
542 winds measured by NOAA's oceanic platforms. Journal of Wind Engineering and Industrial Aerodynamics, 36,
543 pp.381-392.

544 Powell, M.D., Vickery, P.J. and Reinhold, T.A., 2003. Reduced drag coefficient for high wind speeds in tropical
545 cyclones. Nature, 422(6929), pp.279-283.

546 Powell, M., Bowman, D., Gilhousen, D., Murillo, S., Carrasco, N. and St. Fleur, R., 2004. Tropical cyclone winds at
547 landfall: The ASOS–C-MAN wind exposure documentation project. Bulletin of the American Meteorological
548 Society, 85(6), pp.845-851.

549 Rappaport, E.N., 2014. Fatalities in the United States from Atlantic tropical cyclones: New data and interpretation.
550 Bulletin of the American Meteorological Society, 95(3), pp.341-346.

551 Rosenthal, S.L., 1962. A Theoretical Analysis of the Field of Motion in Hurricane Boundary Layer. National
552 Hurricane Research Project Report, p. 12 (56).

553 Schroeder, J.L. and Smith, D.A., 2003. Hurricane Bonnie wind flow characteristics as determined from WEMITE.
554 Journal of Wind Engineering and Industrial Aerodynamics, 91(6), pp.767-789.

555 Schroeder, J.L., Edwards, B.P. and Giammanco, I.M., 2009. Observed tropical cyclone wind flow characteristics.
556 Wind and Structures, 12(4), pp.349-381.

557 Shu, Z.R., Li, Q.S., He, Y.C. and Chan, P.W., 2017. Vertical wind profiles for typhoon, monsoon and thunderstorm
558 winds. Journal of Wind Engineering and Industrial Aerodynamics, 168, pp.190-199.

559 Smith, R.K., 1968. The surface boundary layer of a hurricane. Tellus, 20(3), pp.473-484.

560 Smith, R.K., Montgomery, M.T. and Van Sang, N., 2009. Tropical cyclone spin-up revisited. Quarterly Journal of the
561 Royal Meteorological Society, 135(642), pp.1321-1335.

562 Snaiki, R. and Wu, T., 2017a. A linear height-resolving wind field model for tropical cyclone boundary layer. Journal
563 of Wind Engineering and Industrial Aerodynamics, 171, pp.248-260.

564 Snaiki, R. and Wu, T., 2017b. Modeling tropical cyclone boundary layer: Height-resolving pressure and wind fields.
565 Journal of Wind Engineering and Industrial Aerodynamics, 170, pp.18-27.

566 Sparks, P.R. and Huang, Z., 1999. Wind speed characteristics in tropical cyclones. In Proceedings: 10th International
567 Conference on Wind Engineering.

568 Tse, K.T., Li, S.W., Chan, P.W., Mok, H.Y. and Weerasuriya, A.U., 2013. Wind profile observations in tropical
569 cyclone events using wind-profilers and doppler SODARs. Journal of Wind Engineering and Industrial
570 Aerodynamics, 115, pp.93-103.

571 Tse, K.T., Li, S.W. and Fung, J.C.H., 2014a. A comparative study of typhoon wind profiles derived from field
572 measurements, meso-scale numerical simulations, and wind tunnel physical modeling. Journal of Wind
573 Engineering and Industrial Aerodynamics, 131, pp.46-58.

574 Tse, K.T., Li, S.W., Lin, C.Q. and Chan, P.W., 2014b. Wind characteristics observed in the vicinity of tropical
575 cyclones: An investigation of the gradient balance and super-gradient flow. Wind and Structures, 19(3), pp.249-
576 270.

577 Uhlhorn, E.W., Black, P.G., Franklin, J.L., Goodberlet, M., Carswell, J. and Goldstein, A.S., 2007. Hurricane surface
578 wind measurements from an operational stepped frequency microwave radiometer. Monthly Weather Review,
579 135(9), pp.3070-3085.

580 Vickery, P.J., Wadhera, D., Powell, M.D. and Chen, Y., 2009. A hurricane boundary layer and wind field model for
581 use in engineering applications. Journal of Applied Meteorology and Climatology, 48(2), pp.381-405.

582 Wang, H., and Wu, T., 2017. Gust-Front Factor: A Case Study of Tropical Cyclone-Induced Wind Load Effects on
583 Tall Buildings. In: Proceedings of 13th Americas Conference on Wind Engineering (13ACWE), May, 2017,
584 Gainesville, FL, USA.

585 Weber, R.O., 1999. Remarks on the definition and estimation of friction velocity. Boundary-Layer Meteorology,
586 93(2), pp.197-209.

587 Wieringa, J., 1992. Updating the Davenport roughness classification. Journal of Wind Engineering and Industrial
588 Aerodynamics, 41(1-3), pp.357-368.

589 Wiernga, J., 1993. Representative roughness parameters for homogeneous terrain. Boundary-Layer Meteorology,
590 63(4), pp.323-363.

591 Willoughby, H.E., 1990. Gradient balance in tropical cyclones. Journal of the Atmospheric Sciences, 47(2), pp.265-
592 274.

593 Zhang, J.A., Drennan, W.M., Black, P.G. and French, J.R., 2009. Turbulence structure of the hurricane boundary layer
594 between the outer rainbands. Journal of the Atmospheric Sciences, 66(8), pp.2455-2467.

595 Zhang, J.A. and Uhlhorn, E.W., 2012. Hurricane sea surface inflow angle and an observation-based parametric model.
596 Monthly Weather Review, 140(11), pp.3587-3605.

597 Zilitinkevich, S.S., 1989. Velocity profiles, the resistance law and the dissipation rate of mean flow kinetic energy in
598 a neutrally and stably stratified planetary boundary layer. Boundary-Layer Meteorology, 46(4), pp.367-387.